

Hysteresis and jumps in the $I - V$ curves of disordered two-dimensional materials

Shahar Kasirer* and Yigal Meir†
Physics department, Ben-Gurion University of The Negev
(Dated: December 23, 2021)

The superconductor-insulator transition (SIT) in thin-film disordered superconductors is a hallmark example of a quantum phase transition. Despite being observed more than 30 years ago, its nature is still under a vivid debate. One intriguing observations concerns the insulating side of the transition, which exhibits some unusual properties. Among them is its current-voltage relation ($I - V$ curve), which includes (1) a conductance that changes abruptly by several orders of magnitude with increasing voltage, (2) hysteretic behavior, and (3) multiple (sometimes more than a hundred) smaller current jumps near the transition. Some models have been suggested before, but no model has been successful in accounting for the observed behavior in full. One commonly used approach is to model the disordered sample as a two-dimensional array of conducting islands, where charge carriers tunnel from one island to its neighbors. In those models, fast relaxation is assumed, and the system is treated as always being in electrostatic and thermal equilibrium. Those models are successful in explaining some measurement results, including the phase transition itself, but fail to reproduce hysteresis in their predicted $I - V$ curves. Here, we suggest incorporating finite relaxation time into an array model. We show that, in the slow relaxation limit, our model can reproduce hysteresis and multiple jumps in the $I - V$ curve. Based on our results we argue that a similar behavior should be also observed in two-dimensional normal (non-superconducting) arrays. This claim is supported by past observations. We analyse the role of different parameters in our model, determine the range of relevant time scales in the problem, and compare our results with selected measurements.

I. INTRODUCTION

Phase transitions are ubiquitous in nature, with examples ranging from transformation of solids to liquids to gases, from magnetic to non-magnetic materials, from metals to superconductors, and even from a dense plasma to the current universe [1]. These are examples of *classical phase transition* where the change in phase occurs as a function of temperature. *Quantum phase transitions*, on the other hand, occur at zero temperature, where the ground state of the system changes character when one continuously tunes an external parameter, such as density, magnetic field or chemical compositions [2]. While, in principle, such transitions only occur at zero temperature, they may have important ramifications in a wide range of finite temperatures and physical parameters, a prominent example is the case of high-temperature superconductors [3]. One of the important examples of such a quantum phase transition is the superconducting-insulator transition (SIT) in thin films, where the system changes character from an insulator (extrapolated infinite resistance at zero temperature) to a superconductor (zero extrapolated resistance), as a function of film thickness [4], magnetic field [5] or disorder [6]. Despite being observed more than 30 years ago [4, 5], the nature of SIT is still under debate, due to the interplay between superconductivity and disorder [7]. Of particular interest is the insulating side of the transition: various experiments

indicate persistence of SC correlations into the insulating phase [8–13]. The intriguing nonlinear $I - V$ characteristics in this regime, revealing a conductance that changes by several orders of magnitude with increasing voltage [14–18], has led to a further debate concerning these observations, including the suggestion that this is due to overheating of electrons [16, 19, 20] or the formation of a novel “super-insulator” phase [15, 18]. An example for the intriguing experimental observations is depicted in Fig. 1(b): the current is zero, to experimental accuracy, up to some threshold voltage, and then it rises abruptly. This behavior is, in fact, hysteretic, and the threshold voltage depends on the direction of the voltage tuning. Such data have been obtained both in $a: InO$ [14, 17] and TiN [15, 21] films, though the interpretation of the data was quite different. Even more surprisingly, as can be seen in the same figure, the big jump in the current consists, close to the SIT, of multiple (sometimes more than a hundred [17]) smaller current jumps. Multiple jumps have also been observed in Josephson-junction arrays [22], a system that also exhibits hysteresis (see e.g. [23]). Interestingly, similar data were obtained in a quantum-dot array [24, 25] (Fig. 1(a)), Y_xSi_{1-x} thin films [26] and Au nanocluster films [27], all non SC materials, which suggests a mechanism not limited to superconductors.

An abrupt jump in current can be explained by the overheating model [19]. In this model, when the applied voltage crosses a threshold value, the electron temperature becomes higher than that of the phonons, manifested by a big jump in the $I - V$ curve. Upon decreasing the voltage, electrons stay overheated down to a second threshold voltage, lower than the first one, leading to hysteresis in the observed curve. Although this

* kasirer@mail.tau.ac.il; Biochemistry Department & Raymond and Beverly Sackler School of Physics and Astronomy, Tel-Aviv University

† ymeir@bgu.ac.il

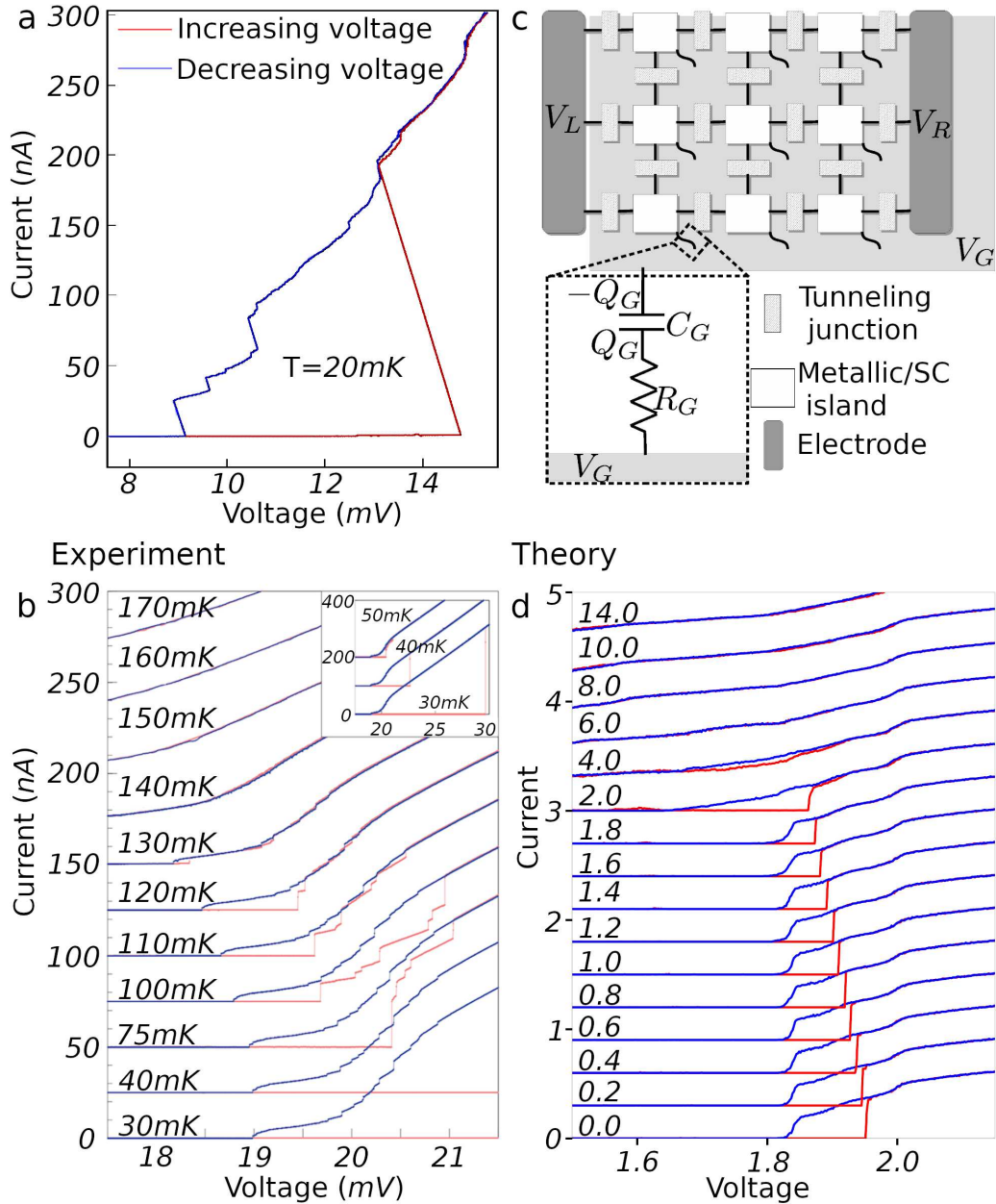


Figure 1. (a) Experimental $I - V$ curves of a GaAs quantum dot array [24]. (b) Experimental $I - V$ curves of an $a: \text{InO}$ sample in the insulating phase, near the superconductor-insulator transition, for different temperatures. Curves are offset from one another by 25nA . Inset: Expanded V -range for the low temperature results [17]. (c) The 2 dimensional island array model: charge carriers can tunnel from one island to its neighbors, through the tunneling junctions. Each tunneling junction is attributed a tunneling-resistance and capacitance. Each island is coupled to the gate of voltage V_G , via an RC circuit (inset shows enlarged view of this coupling). (d) Simulated $I - V$ curves of a 10×10 array model, for different temperatures. Temperature, voltage and current are expressed in units of $e^2/(k_B \langle C \rangle) \cdot 10^{-3}$, $e/\langle C \rangle$ and $e/\langle \langle R \rangle C \rangle$, respectively. $\langle C \rangle$ and $\langle R \rangle$ are the average tunneling junctions capacitance and resistance, respectively. Curves are offset from one another by $0.3e/\langle \langle R \rangle C \rangle$. Simulation parameters: $V_{max} = 2.4 \langle C \rangle / e$, $V_G = 0$, $R_G = 50 \langle R \rangle$, $C_G = 5 \langle C \rangle$, $\sigma_C = 0.05 \langle C \rangle$, $\sigma_R = 0.9 \langle R \rangle$.

model is successful in reproducing the abrupt jump and the hysteresis in the $I - V$ curve, it cannot account for multiple current jumps. An alternative model is based on the observation that disorder breaks the system into “islands” with higher SC order parameter, separated by “insulating” areas where the SC order is weak [28–30] (such

spatial fluctuations in the SC gap have indeed been observed experimentally [10, 18, 31, 32]). In such a model one would expect a threshold voltage, due to Coulomb blockade, and even multiply current jumps due to opening of new parallel transport channels, or allowing multiple occupation states of the islands. Indeed, previous

calculations of the current-voltage characteristics in normal arrays gave rise to a threshold voltage [33–35] and even multiple jumps [36, 37]. Similar threshold behavior in the insulating phase has also been observed in simulations of Josephson-junction arrays [38, 39]. However, none of the array simulations exhibited the hysteresis observed in the experiment. Accordingly, none of the existing theories can explain the combined experimental observations of threshold and one or multiple jumps in the $I - V$ curve, adding to the enigma of the nature of the insulating state close to the SIT. Here we build upon the model of a disordered array, and demonstrate how, by incorporating the physically relevant relaxation time (see below), one can explain, within a single model, the occurrence of hysteresis, jumps and threshold voltage in this system.

II. SUGGESTED MODEL

When one considers transport of electrons or Cooper pairs through the array, there are three important time scales: (1) the tunneling time between islands, (2) the inter-tunneling time - the time between tunneling events, and (3) the relaxation time - how fast an array restores electrostatic and thermal equilibrium after a tunneling event has occurred. In most existing array models, both tunneling and relaxation time scales are assumed to be much shorter than the inter-tunneling time, and thus are treated as instantaneous. While this assumption is justified for the tunneling time, which is usually the fastest time scale in the system, the relaxation time depends on various sample parameters, such as capacitance and resistance to the gates or the substrate. If it is much longer than the inter-tunneling time, one cannot assume that the system is always in electrostatic equilibrium. Below we show that in this “slow relaxation limit”, one can reproduce the main features in the experimental $I - V$ curve.

Since the physics we describe also applies to normal arrays, we first start with this simpler system [33, 34, 40]. The electrostatic energy of a 2-dimensional islands array (Fig. 1(c)) is given by

$$E = \sum_{i \in \text{islands}} \left[\frac{C_G}{2} (V_i - V_G)^2 + \sum_{j \in \text{neighbors of island } i} \frac{C_{ij}}{4} (V_i - V_j)^2 \right] + \sum_{x \in \text{electrodes}} \left[Q_x V_x + \sum_{j \in \text{neighbors of electrode } x} \frac{C_{xj}}{2} (V_x - V_j)^2 \right] \quad (1)$$

where V_i, V_x, V_G are the electric potentials on island i , electrode x (left or right) and the gate, respectively, Q_x is the charge on electrode x and C_{ij} is the capacitance of the tunneling junction connecting islands i and j . The factor of 1/4 in front of the second term is there to avoid double counting. To calculate the current through our sample, we would be interested in the change in energy resulting

from a tunneling event. For an electron tunneling from island i to island j , the change in electrostatic energy can be presented in a simple form [40]

$$\Delta E^{i \rightarrow j} = \frac{e}{2} [(V_j - V_i) + (V'_j - V'_i)] \quad (2)$$

where V_i and V'_i are the electric potentials on island i before and after tunneling respectively. To relate the electric potential on each island to the charge on it, we define the capacitance matrix \mathcal{C} .

$$\mathcal{C}_{i,j} = \begin{cases} \sum_{\substack{k \in \text{neighbors of} \\ \text{island } i}} C_{i,k} & \text{if } i = j \\ -C_{ij} & \text{if island } i \text{ and } j \text{ are neighbors} \\ 0 & \text{otherwise} \end{cases} \quad (3)$$

With this definition, and using simple charge continuity considerations, the local electric potential on each island can be written as

$$\mathbf{V} = \mathcal{C}^{-1} (e\mathbf{n}' + \mathbf{Q}_G) \quad (4)$$

Where \mathbf{V} is a column vector with V_i as its entries and the entries of \mathbf{n}' are defined by

$$en'_i = \begin{cases} en_i + C_{ix} V_x & \text{island } i \text{ is a neighbor of electrode } x \\ en_i & \text{otherwise} \end{cases} \quad (5)$$

where n_i is the number of charge carriers on island i . \mathbf{Q}_G holds the charge on each gate capacitor (with sign convention as indicated in Fig. 1(c)). Using Eq. (2–5) and treating the tunneling of charge carriers between neighboring islands as a small perturbation, the tunneling rates are given by [41]:

$$\Gamma(\Delta E) = \frac{1}{e^2 R_T} \frac{-\Delta E}{1 - \exp(\Delta E/k_B T)} \quad (6)$$

Where R_T is the tunneling resistance between the islands, and ΔE is the electrostatic energy difference between the charge configurations before and after the tunneling event. For low temperatures tunneling will only occur if $\Delta E < 0$, namely when the voltage difference between the islands is large enough to compensate for the additional Coulomb energy. Indeed these previous calculations, which assumed that the charges instantaneously relax to their lowest-energy configuration after the tunneling event, found that this Coulomb blockade leads to a threshold voltage below which current cannot flow through the system [33].

As mentioned above, the assumption of instantaneous relaxation precludes hysteresis and thus these models cannot explain some of the observations. The importance of a finite relaxation time has been pointed out by Korotkov [42], who showed that for a single island, finite relaxation time may lead to hysteresis. Here we allow for such finite relaxation time by connecting each island

to a gate or substrate, by an RC circuit (dotted square in Fig. 1c). This RC coupling is what determines the charge dynamics between tunneling events. To find the equations describing this process, we calculate the electric potential on each island by its voltage difference from the gate

$$V_i = V_G - [\mathbf{R}_G]_i \left[\frac{d\mathbf{Q}_G}{dt} \right]_i - \frac{1}{[C_G]_i} [\mathbf{Q}_G]_i \quad (7)$$

Solving Eq. (4,7) for $d\mathbf{Q}_G/dt$, we find the following differential equations

$$\begin{aligned} \frac{d\mathbf{Q}_G}{dt} &= \mathcal{T}^{-1} (\mathbf{Q}_G - \mathbf{Q}_n) \\ [\mathcal{T}^{-1}]_{ij} &\equiv \frac{1}{[\mathbf{R}_G]_i} \left([\mathcal{C}^{-1}]_{i,j} + \frac{1}{[C_G]_i} \delta_{i,j} \right) \\ [\mathbf{Q}_n]_i &\equiv \frac{1}{[\mathbf{R}_G]_i} \sum_j [\mathcal{T}]_{ij} \left(V_G \delta_{ij} + \frac{1}{[C_G]_j} en'_j \right) - en'_i \quad (8) \end{aligned}$$

We can obtain a numerical solution for this linear system of ODEs, via diagonalization of \mathcal{T} , and use it to calculate the dynamics of charge distribution between tunnelings.

For the simulation results presented here, we used the same gate resistance and capacitance for all islands. From Eqs. (6,8), the ratio of the relaxation time to the inter-tunneling time is determined by the ratio of gate resistance R_G to the tunneling resistances R_T . Therefore, in the limit where R_G is much bigger than all relevant tunneling resistances, one cannot employ the instantaneous relaxation assumption, used in previous calculations. In the following, we incorporate this finite relaxation time in the simulations. Assuming that the time between consecutive measurements is much longer than the relaxation time, we can ignore the relaxation dynamics and calculate only the steady state solution for the current in our model. To do that we used Kinetic Monte-Carlo simulations [43]. Charge distribution was updated between tunneling events, according to Eq. (8). To calculate $I - V$ curves, we ran the simulation for each value of the external voltage, until reaching a steady state (which was verified by checking that the average charge distribution is constant), and then the steady-state current was calculated. We then proceed to running the simulation for the next voltage value, while keeping the charge distribution as it was at the end of the previous run.

III. RESULTS

A. A Single Island

In order to understand the role of the different parameters, let us first study a simple system, consisting of a single conducting island (see inset in Fig. 2(b)), for which one can also obtain analytical results for $T = 0$ (For detailed analytical solution see Appendix A). These results and simulation results for $T > 0$ are presented in Fig. 2. Comparing results for an island with and without asymmetry between the left and right tunneling resistances

(Fig. 2(a,b) vs. 2(c,d)), we conclude that, in order to get visible hysteresis and current jumps, we need tunneling resistance asymmetry ($R_L \neq R_R$). In addition, for the cases with hysteresis, we see that the hysteresis loop area becomes bigger when C_G increases (Fig. 2(c) vs. 2(d)). As temperature increases, the area of each hysteresis loop becomes smaller, and the $I - V$ curves become smoother. A similar thing happens when increasing the applied voltage. It is encouraging to note that these results qualitatively resemble the experimental $I - V$ curves for a single quantum dot [24]. We can understand those results intuitively in the following way: Tunneling resistance asymmetry will control the average number of charge carriers in the system. For example, if $R_R > R_L$ it would be easier for carriers to tunnel into the island from the left electrode, than it is to tunnel from the island to the right electrode, and the average number of carriers on the island would grow with the external voltage. This would, in turn, change Q_G which is the slow degree of freedom that acts as a memory in our system. Increasing C_G , in addition, would enable more steady-state solutions for Q_G and thus more jumps and larger hysteresis loops (See Appendix A).

B. Normal Array

Following the single island results, we used our simulation to calculate $I - V$ curves for normal disordered arrays with large gate capacitance ($C_G > \langle C \rangle$). Disorder was realized by choosing, for each junction, random tunneling resistance and capacitance (resistance and capacitance values distributes as e^α where α is a uniform random variable). Examples of the results are shown in Fig. 1(d), where both hysteresis and jumps are evident. Moreover, in agreement with the low-temperature experimental results, the threshold voltage for increasing voltage is temperature dependent, while the one for decreasing voltage is not.

For a single island, we saw that tunneling resistance asymmetry had a significant effect on hysteresis area. Therefore, it is natural to assume that tunneling resistance disorder would have a similar effect on hysteresis area in arrays. To check this, we ran our simulations for different disorder realizations. We then grouped together realizations with similar standard-deviation for the tunneling resistance distribution (at least 10 realizations at each group). For each group we calculated the average hysteresis area, and threshold voltages (both for increasing and decreasing applied voltage). The results are plotted in Fig. 3. Indeed, as could be expected from the single island results, hysteresis area increases with disorder. Interestingly, the threshold voltage also drops when disorder increases (despite being resistance independent for a single island). As disorder increases, the difference between the threshold voltages for increasing and decreasing voltages tend to increase, matching the increase in hysteresis area. This is more apparent for the small ar-

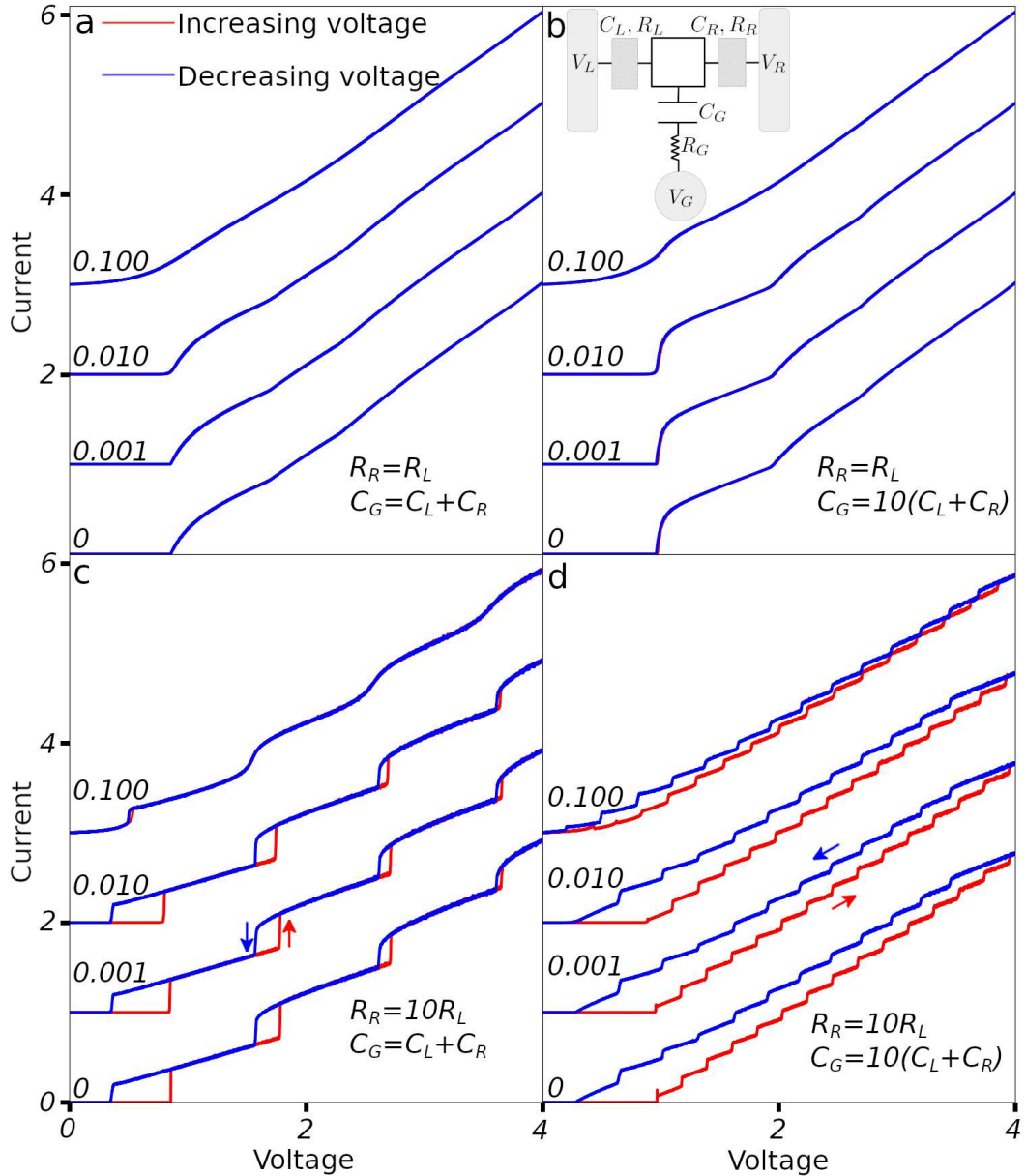


Figure 2. Simulated single island I-V curves, for different temperatures (temperature is indicated above each curve). Temperature, voltage and current are expressed in units of $e^2 / (k_B \langle C \rangle)$, $e / \langle C \rangle$ and $e / (\langle R \rangle \langle C \rangle)$, respectively. Curves for different temperatures are offset from one another by $e / (\langle R \rangle \langle C \rangle)$. (a) Small gate capacitance and equal resistance for both junctions. (b) Large gate capacitance and equal resistance. Inset - Single island model schema. (c) Small gate capacitance and asymmetric tunneling resistance. (d) Large gate capacitance and asymmetric resistance. Simulation parameters: $C_L = 2C_R$, $V_G = 0$, $R_G = 1000(R_L + R_R)$.

rays (Fig. 3(a)) than it is for the larger ones (Fig. 3(b)).

Next we checked the effect of temperature. In Fig. 1(d), we compare I-V curves, of the same 10×10 array realization, for different temperatures. As temperature increases, threshold voltage and hysteresis loop area become smaller. The big hysteresis loop we see for small temperatures diminishes when temperature rises, and we are left with smaller loops, which also disappear for even higher temperatures. These results are in qualitative agreement with the experimental results from [17] (Fig.

1(b)).

C. Superconducting Array

Having demonstrated that incorporating a finite relaxation time in calculations of the transport through a random normal array is able to explain the experimental observations of threshold, multiple jumps and hysteresis, we next checked how these results are modified when

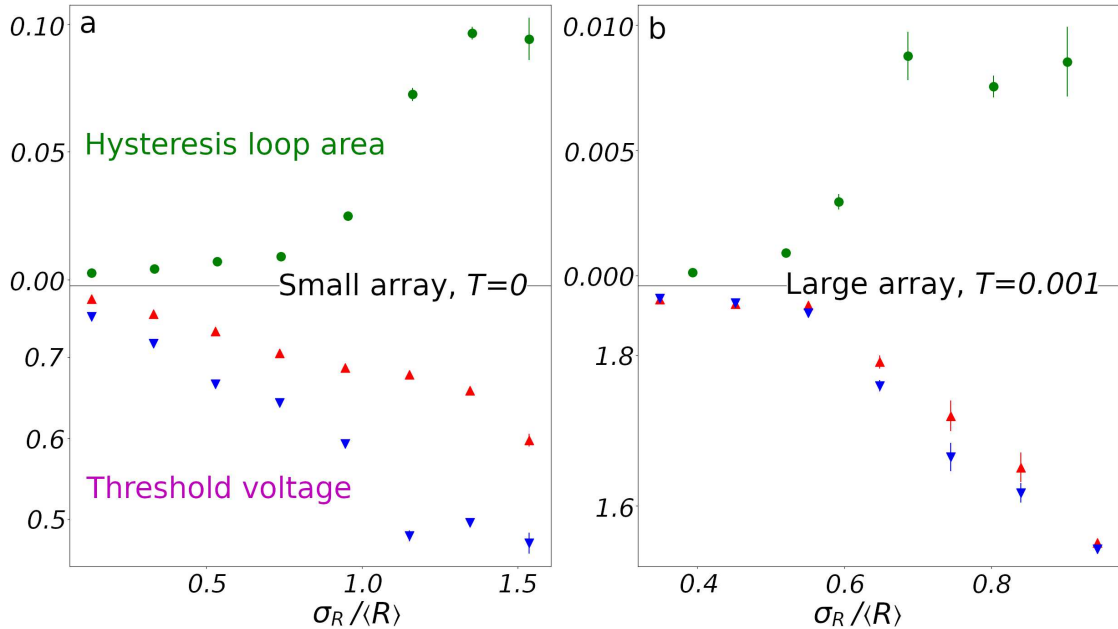


Figure 3. Hysteresis loop area and threshold voltages as a function of resistance disorder. Calculated by averaging the results from > 10 different array realizations, with various tunneling capacitance disorder values, for each data point. Error bars show standard error of averages. Upwards pointing red triangles - increasing voltage. Downwards pointing blue triangles - decreasing voltage. Temperature, loops areas and threshold voltages are expressed in units of $e^2 / (k_B \langle C \rangle)$, $e^2 / (\langle C \rangle^2 \langle R \rangle)$ and $e / \langle C \rangle$, respectively. (a) For 3×3 arrays at $T = 0$. (b) For 10×10 arrays at $k_B T = 10^{-3} \cdot e^2 / \langle C \rangle^2$. Common simulation parameters: $V_G = 0$, $R_G = 100 \langle R \rangle$, $C_G = 10 \langle C \rangle$.

considering transport through a superconducting array. In this case both quasi-particles and Cooper-pairs can, in principle, tunnel between the islands, and one has to take into account their different statistics and density-of-states. The resulting tunneling rates are [41]

$$\Gamma_{cp}(\Delta E) = \frac{\pi}{2\hbar} E_J^2 P_2(-\Delta E), \quad (9)$$

for Cooper-pairs, where E_J is Josephson's energy, obtained from Δ using the standard relation [44] and $P_\kappa(E)$ is the probability of absorbing energy E by the environment, $\kappa = 1$ for quasi-particles and 2 for Cooper-pairs. For quasi-particles

$$\Gamma_{qp}(\Delta E) = \frac{1}{e^2 R} \int_{-\infty}^{\infty} dE \int_{-\infty}^{\infty} dE' \frac{N_s(E)N_s(E' - \Delta E)}{N(0)^2} \times f(E) [1 - f(E' - \Delta E)] P_1(E - E'), \quad (10)$$

where $f(E)$ is Fermi-Dirac distribution. $N_s(E) / N(0)$ is the BCS quasi-particle density of states, which is given by [45]

$$\frac{N_s(E)}{N(0)} = \begin{cases} \frac{|E|}{\sqrt{E^2 - \Delta^2}} & |E| > \Delta \\ 0 & |E| < \Delta \end{cases} \quad (11)$$

For a high impedance environment, where the perturbation theory leading to Eq. 9 is valid, $P_\kappa(E)$ is given by [41]

$$P_\kappa(E) = \frac{\exp \left[- (E - \kappa^2 E_c)^2 / 4\kappa^2 E_c k_B T \right]}{\sqrt{4\pi \kappa^2 E_c k_B T}} \quad (12)$$

where E_c is the charging energy of the environment.

Tunneling rates were calculated, in a similar way to [46], assuming that energy is absorbed by the intrinsic impedance of the array. In that case, the dominant impedance comes from the gate coupling (R_G in the slow relaxation limit) and the environment's charging energy (E_c in Eq. 12) is given by $e^2 / 2C_G$. The calculated tunneling rates are plotted in Fig. 4(a). Cooper-pair tunneling rates (solid curves) are centered around $(-\Delta E) \approx 4E_c$ which is the energy that is best absorbed by the intrinsic impedance (see eq. 12). Quasi-particles require $(-\Delta E) > \max[2\Delta, E_c]$, to overcome the SC gap and, in addition, to compensate for the energy that is absorbed by the intrinsic impedance (dashed curves). For larger energy gains, rates grow linearly, in a similar way to the tunneling rates of electrons in normal arrays (purple dotted curve). For $\Delta \approx 2E_c$, both cooper pairs and quasi-particles tunneling would give a significant contribution to the current. For $\Delta \ll E_c$, only quasi particles would contribute to the current.

We incorporated these tunneling rates into our simulation, to calculate the current through SC arrays. The resulted I-V curves, for a 5×5 , array are plotted in Fig. 4(b). For all superconducting gap values we see hysteresis and jumps. Increasing Δ , threshold voltage increases and we see a bigger current jump when external voltage is increased above it.

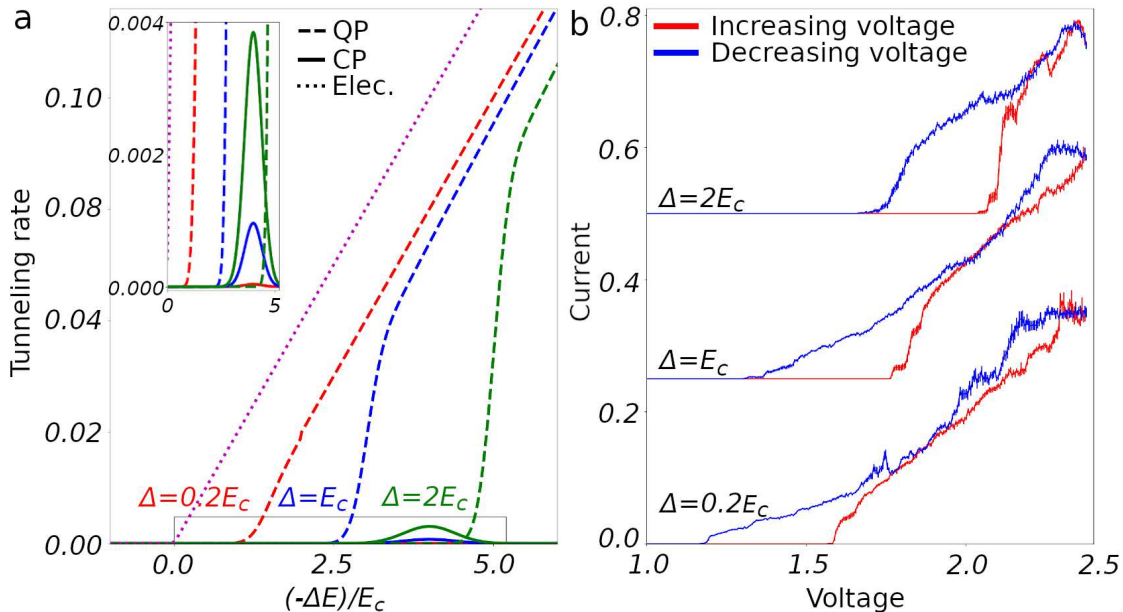


Figure 4. (a) Tunneling rates for Cooper-pairs (solid lines) and quasi-particles (dashed lines), for different superconducting gaps. The tunneling rates for electrons (dotted line) are plotted for comparison. Inset - Close-up view of the marked region. Tunneling rates are expressed in units of $1/\langle\langle R \rangle\langle C \rangle \rangle$. (b) $I - V$ curves for a 5×5 superconducting array, with different superconducting gaps. Error-bars indicate standard errors. Voltage and current are expressed in units of $e/\langle C \rangle$ and $e/\langle\langle R \rangle\langle C \rangle \rangle$, respectively. Curves are shifted up by $0.25e/\langle\langle R \rangle\langle C \rangle \rangle$ from each other. Simulation parameters: $k_B T = 0.4 \cdot 10^{-3} e^2/\langle C \rangle$, $E_c = 25 \cdot 10^{-3} e^2/\langle C \rangle$, $V_{max} = 2.4 \langle C \rangle/e$, $V_G = 0$, $R_G = 234 \langle R \rangle$, $C_G = 21 \langle C \rangle$, $\sigma_C = 0.64 \langle C \rangle$, $\sigma_R = 0.78 \langle R \rangle$.

IV. CONCLUSION

In this paper we have introduced a new ingredient into the physics of disordered systems - a slow relaxation of some of the degrees of freedom, in this case the charge distribution, towards electrostatic equilibrium. It has been demonstrated that including this new ingredient into a random array model explains the puzzling observations of hysteresis and multiple current jumps in $I - V$ curves in disordered superconductors near the superconductor-insulator transition, and in quantum-dot arrays, thereby adding an important tier to our understanding of disordered quantum systems in general. For a crude estimation of the required relaxation time to satisfy our model's assumptions we used the measured current in [17, 24] to estimate an average inter-tunneling time of $\sim 10^{-10} - 10^{-12}$ sec. This means that the relaxation time should be at least an order of magnitude longer, at least a nanosecond, and the measuring frequency should be much slower than a GHz to always measure a steady state. The relaxation time scale could be determined by the coupling (e.g. resistance and capacitance) between the sample and the substrate or gates. Since this is usually uncontrolled in experiments, it may explain why some samples show hysteresis and jumps, while others, nomi-

nally with the same parameters, do not (see, e.g. [47]). Another possible source of slow dynamics may be two-level systems, which have already been observed [48, 49] in similar disordered SC films. It would be interesting, though experimentally challenging, to control the relaxation rate and check the predictions of our theory, showing, for example, the suppression of the hysteretic behavior for a short relaxation time. Our results point out the importance of different time-scales in such disordered strongly-interacting system and offer a novel viewpoint: the system might not be in thermal and electrostatic equilibrium but rather in a new type of a steady state, depicted by the slow degree of freedom in the system. Our model, and simulation method, can be used as a basis for future research on disordered materials where relaxation cannot be considered instantaneous. In addition, the approach we used, i.e. adding a slow degree of freedom to account for hysteresis in a system, might be applicable to other, possibly hysteretic disordered systems [50].

ACKNOWLEDGMENTS

The authors acknowledge useful discussions with N. S. Wingreen, L. Zhu, B. Weiner and A. Erez. This work was supported by the Israel Science Foundation (grant 3523/2020).

-
- [1] N. Goldenfeld, *Lectures on phase transitions and the renormalization group* (CRC Press, 2018).
- [2] S. L. Sondhi, S. M. Girvin, J. P. Carini, and D. Shahar, Continuous quantum phase transitions, *Rev. Mod. Phys.* **69**, 315 (1997).
- [3] F. F. Balakirev, J. B. Betts, A. Migliori, I. Tsukada, Y. Ando, and G. S. Boebinger, Quantum phase transition in the magnetic-field-induced normal state of optimum-doped high- t_c cuprate superconductors at low temperatures, *Physical review letters* **102**, 017004 (2009).
- [4] D. B. Haviland, Y. Liu, and A. M. Goldman, Onset of superconductivity in the two-dimensional limit, *Physical Review Letters* **62**, 2180 (1989).
- [5] A. F. Hebard and M. A. Paalanen, Magnetic-field-tuned superconductor-insulator transition in two-dimensional films, *Physical Review Letters* **65**, 927 (1990).
- [6] T. I. Baturina, A. Bilušić, A. Y. Mironov, V. M. Vinokur, M. R. Baklanov, and C. Strunk, Quantum-critical region of the disorder-driven superconductor-insulator transition, *Physica C: Superconductivity Proceedings of the Workshop on Fluctuations and Phase Transitions in Superconductors*, **468**, 316 (2008).
- [7] A. M. Goldman, SUPERCONDUCTOR-INSULATOR TRANSITIONS, *International Journal of Modern Physics B* **24**, 4081 (2010).
- [8] D. Kowal and Z. Ovadyahu, Disorder induced granularity in an amorphous superconductor, *Solid State Communications* **90**, 783 (1994).
- [9] R. W. Crane, N. P. Armitage, A. Johansson, G. Sambandamurthy, D. Shahar, and G. Grüner, Fluctuations, dissipation, and nonuniversal superfluid jumps in two-dimensional superconductors, *Physical Review B* **75**, 094506 (2007).
- [10] B. Sacepe, C. Chapelier, T. I. Baturina, V. M. Vinokur, M. R. Baklanov, and M. Sanquer, Disorder-induced inhomogeneities of the superconducting state close to the superconductor-insulator transition, *Physical Review Letters* **101**, 157006 (2008).
- [11] K. H. S. B. Tan, K. A. Paredo, and A. M. Goldman, Evidence of spatially inhomogeneous pairing on the insulating side of a disorder-tuned superconductor-insulator transition, *Physical Review B* **78**, 014506 (2008).
- [12] H. Q. Nguyen, S. M. Hollen, M. D. Stewart, J. Shainline, A. Yin, J. M. Xu, and J. M. Valles, Observation of giant positive magnetoresistance in a cooper pair insulator, *Physical Review Letters* **103**, 157001 (2009).
- [13] A. Kamlapure, M. Mondal, M. Chand, A. Mishra, J. Jesudasan, V. Bagwe, L. Benfatto, V. Tripathi, and P. Raychaudhuri, Measurement of magnetic penetration depth and superconducting energy gap in very thin epitaxial NbN films, *Applied Physics Letters* **96**, 072509 (2010).
- [14] G. Sambandamurthy, L. W. Engel, A. Johansson, and D. Shahar, Superconductivity-related insulating behavior, *Physical Review Letters* **92**, 107005 (2004).
- [15] V. M. Vinokur, T. I. Baturina, M. V. Fistul, A. Y. Mironov, M. R. Baklanov, and C. Strunk, Superinsulator and quantum synchronization, *Nature* **452**, 613 (2008).
- [16] M. Ovadia, B. Sacépé, and D. Shahar, Electron-phonon decoupling in disordered insulators, *Physical Review Letters* **102**, 176802 (2009).
- [17] O. Cohen, M. Ovadia, and D. Shahar, Electric breakdown effect in the current-voltage characteristics of amorphous indium oxide thin films near the superconductor-insulator transition, *Physical Review B* **84**, 100507(R) (2011).
- [18] T. I. Baturina and V. M. Vinokur, Superinsulator-superconductor duality in two dimensions, *Annals of Physics* **331**, 236 (2013).
- [19] B. L. Altshuler, V. E. Kravtsov, I. V. Lerner, and I. L. Aleiner, Jumps in current-voltage characteristics in disordered films, *Physical Review Letters* **102**, 176803 (2009).
- [20] T. Levinson, A. Doron, I. Tamir, G. C. Tewari, and D. Shahar, Direct determination of the temperature of overheated electrons in an insulator, *Physical Review B* **94**, 174204 (2016).
- [21] T. I. Baturina, A. Y. Mironov, V. M. Vinokur, M. R. Baklanov, and C. Strunk, Localized superconductivity in the quantum-critical region of the disorder-driven superconductor-insulator transition in TiN thin films, *Physical Review Letters* **99**, 257003 (2007).
- [22] P. Delsing, C. D. Chen, D. B. Haviland, Y. Harada, and T. Claeson, Charge solitons and quantum fluctuations in two-dimensional arrays of small josephson junctions, *Physical Review B* **50**, 3959 (1994).
- [23] C. G. L. Böttcher, F. Nichele, M. Kjaergaard, H. J. Suominen, J. Shabani, C. J. Palmstrøm, and C. M. Marcus, Superconducting, insulating and anomalous metallic regimes in a gated two-dimensional semiconductor-superconductor array, *Nature Physics* **14**, 1138 (2018).
- [24] C. I. Duruöz, R. M. Clarke, C. M. Marcus, and J. S. Harris, Conduction threshold, switching, and hysteresis in quantum dot arrays, *Physical Review Letters* **74**, 3237 (1995).
- [25] N. E. Staley, N. Ray, M. A. Kastner, M. P. Hanson, and A. C. Gossard, Electric-field-driven insulating-to-conducting transition in a mesoscopic quantum dot lattice, *Physical Review B* **90**, 195443 (2014).
- [26] F. Ladieu, M. Sanquer, and J. P. Bouchaud, Depinning transition in mott-anderson insulators, *Physical Review B* **53**, 973 (1996).
- [27] M. G. Ancona, W. Kruppa, R. W. Rendell, A. W. Snow, D. Park, and J. B. Boos, Coulomb blockade in single-layer au nanocluster films, *Physical Review B* **64**, 033408 (2001).
- [28] A. Ghosal, M. Randeria, and N. Trivedi, Role of spatial amplitude fluctuations in highly disordered s-wave superconductors, *Physical Review Letters* **81**, 3940 (1998).
- [29] A. Ghosal, M. Randeria, and N. Trivedi, Inhomogeneous pairing in highly disordered s-wave superconductors, *Physical Review B* **65**, 014501 (2001).
- [30] Y. Dubi, Y. Meir, and Y. Avishai, Nature of the superconductor-insulator transition in disordered superconductors, *Nature* **449**, 876 (2007).
- [31] B. Sacepe, T. Dubouchet, C. Chapelier, M. Sanquer, M. Ovadia, D. Shahar, M. Feigel'man, and L. Ioffe, Localization of preformed cooper pairs in disordered superconductors, *Nature Physics* **7**, 239 (2011).
- [32] M. Chand, G. Saraswat, A. Kamlapure, M. Mondal, S. Kumar, J. Jesudasan, V. Bagwe, L. Benfatto, V. Tripathi, and P. Raychaudhuri, Phase diagram of the

- strongly disordered s-wave superconductor NbN close to the metal-insulator transition, *Physical Review B* **85**, 014508 (2012).
- [33] A. A. Middleton and N. S. Wingreen, Collective transport in arrays of small metallic dots, *Physical Review Letters* **71**, 3198 (1993).
- [34] Y. Enomoto, Charge glass transition in disordered two-dimensional arrays of mesoscopic grains, *Physica B: Condensed Matter* **272**, 64 (1999).
- [35] D. M. Kaplan, V. A. Sverdlov, and K. K. Likharev, Coulomb gap, coulomb blockade, and dynamic activation energy in frustrated single-electron arrays, *Physical Review B* **68**, 045321 (2003).
- [36] H.-O. Müller, K. Katayama, and H. Mizuta, Effects of disorder on the blockade voltage of two-dimensional quantum dot arrays, *Journal of Applied Physics* **84**, 5603 (1998).
- [37] S. Jha and A. A. Middleton, Effects of disorder on electron transport in arrays of quantum dots, *arXiv:cond-mat/0511094* (2005).
- [38] V. A. Otterlo, P. A. Bobbert, and G. Schön, Charge dynamics in junction arrays, *Helvetica Physica Acta* **65**, 379 (1992).
- [39] D. Reinel, W. Dieterich, T. Wolf, and A. Majhofer, Flux-flow phenomena and current-voltage characteristics of josephson-junction arrays with inductances, *Physical Review B* **49**, 9118 (1994).
- [40] N. S. Bakhvalov, G. S. Kazacha, K. K. Likharev, and S. I. Serdyukova, Statics and dynamics of single-electron solitons in two-dimensional arrays of ultrasmall tunnel junctions, *Physica B: Condensed Matter* **173**, 319 (1991).
- [41] G. L. Ingold and Y. V. Nazarov, Charge tunneling rates in ultrasmall junctions, in *Single Charge Tunneling: Coulomb Blockade Phenomena In Nanostructures*, NATO ASI Series, edited by H. Grabert and M. H. Devoret (Springer US, 1992) pp. 21–107.
- [42] A. N. Korotkov, Single-electron transistor controlled with a RC circuit, *Physical Review B* **49**, 16518 (1994).
- [43] D. T. Gillespie, Exact stochastic simulation of coupled chemical reactions, *The Journal of Physical Chemistry* **81**, 2340 (1977).
- [44] M. Tinkham, *Introduction to superconductivity* (Courier Corporation, 2004).
- [45] J. Bardeen, L. N. Cooper, and J. R. Schrieffer, Theory of Superconductivity, *Physical Review* **108**, 1175 (1957).
- [46] J. H. Cole, J. Leppäkangas, and M. Marthaler, Correlated transport through junction arrays in the small Josephson energy limit: incoherent Cooper-pairs and hot electrons, *New Journal of Physics* **16**, 063019 (2014).
- [47] A. Doron, T. Levinson, F. Gorniacyzk, I. Tamir, and D. Shahar, The critical current of disordered superconductors near 0 k, *Nature Communications* **11**, 2667 (2020).
- [48] S. Wissberg, A. Frydman, and B. Kalisky, Local view of superconducting fluctuations, *Applied Physics Letters* **112**, 262602 (2018).
- [49] A. Kremen, H. Khan, Y. L. Loh, T. I. Baturina, N. Trivedi, A. Frydman, and B. Kalisky, Imaging quantum fluctuations near criticality, *Nature Physics* **14**, 1205 (2018).
- [50] Our simulation is written in Python and is available as an open-source code at https://github.com/kasirershaharbgu/random_2D_tunneling_arrays.

Appendix A: Single island at zero temperature - analytic solution

In the case of a single island in zero temperature (see schematic in, Fig. 2), we can represent the possible states and transitions of our system in a simple graph in which each state is represented by a vertex and the weigh of each directed edge is the matching transition rate (e.g. Fig. A.1). We would like to find the probability to find the system in each state. To do so, we define the out-flow from each vertex to be its probability times the sum of all its out-going edges' weights. We define the in-flow to a vertex as the sum of out-flows from all vertices which have an edge from them to that vertex. In a steady state, the in-flow and out-flow of each vertex are equal. For a given Q_G and V , one can find the steady state solution using the following procedure. First, an initial probability is assigned to an edge vertex (e.g. $n = \pm 2$ in Fig. A.1). Then other probabilities are calculated such that the in-flow and out-flow are equal for each vertex, starting from the chosen vertex and gradually going to the opposite side of the graph. Finally, the probabilities are normalized such that their sum would be 1. Having calculated the steady state probability, we can calculate the average current by

$$I(Q_G, V) = -e \sum_n p(n) [\Gamma_L^+(n) - \Gamma_L^-(n)] \\ = -e \sum_n p(n) [\Gamma_R^-(n) - \Gamma_R^+(n)] \quad (A.1)$$

Notice that the steady state probability and the tunneling rates depend both on Q_G and V .

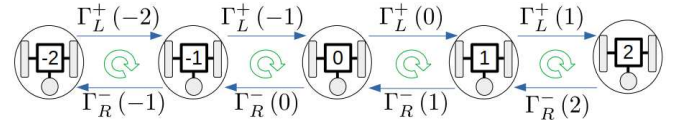


Figure A.1. Single island possible states graph representation. Calculated for $C_L = C_R, V_G = 0$ and small external voltage. Each vertex represents an occupation state. The number of excess carriers on the island is indicated for each state. Edges connect neighboring states, the weight of each corresponds to the matching tunneling rate. Γ_x^+, Γ_x^- are the rates for adding or removing one electron from the island from/to electrode x , respectively. Green arrows show cycles for which 1 electron charge passes from left to right.

The resulting current depends on Q_G . For slow relaxation, Q_G will relax to its mean equilibrium value. In that case, the solution for Eq. 8 would be

$$Q_G(n, t) = \left(Q_0 - \langle Q_n \rangle_{Q_G} \right) e^{-\frac{t}{\tau}} + \langle Q_n \rangle_{Q_G} \\ \langle Q_n \rangle_{Q_G} \equiv \sum_n p_{Q_G}(n, V) Q_n(V) \quad (A.2)$$

The Q_G subscript is there to remind us that the steady state probability, and hence also all averages, depend on

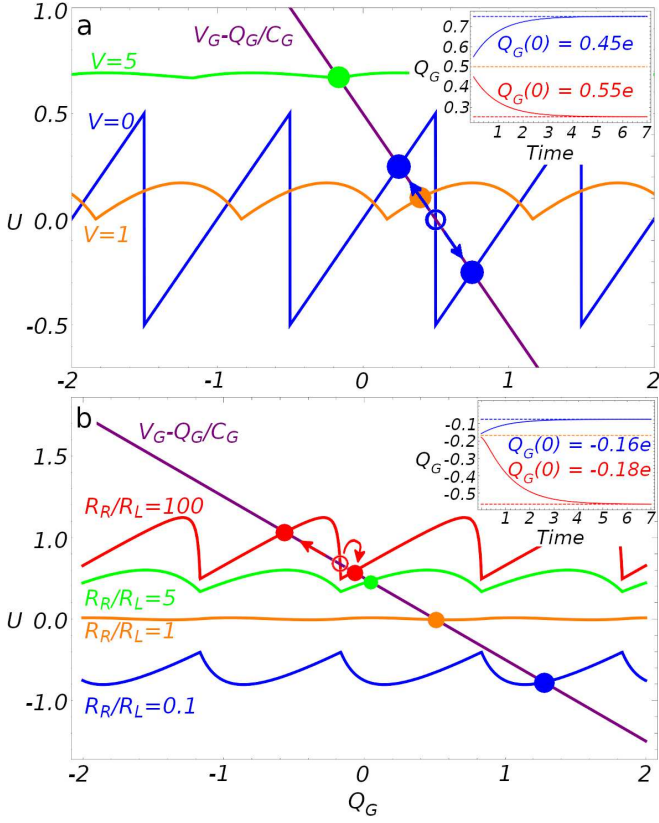


Figure A.2. Average voltage on island for different external voltages (a) and resistances (b). Stable steady state solutions are marked with a whole circle, unstable with an empty circle. Small arrows indicate direction of convergence for bi-stable cases ($V = 0$ in (a) and $R_R/R_L = 100$ in (b)). Voltages are expressed in units of $\frac{e}{C_L+C_R}$. (a) For $V = 0$, the shape is saw-tooth like. For large V , average U approaches a Q_G independent solution. (b) As resistances ratio, R_R/R_L , increases, $\langle U \rangle_{Q_G}$ shape resembles the $V = 0$ result. For $R_L > R_R$ the result is mirrored about the x -axis. Insets - Q_G for bi-stable cases, as a function of time, for different initial values. Dashed lines mark the steady state solutions (red and blue - stable, orange - unstable). Mutual parameters: $C_R = 2C_L$, $C_G = C_L + C_R$, $V_L = -V_R$, $V_G = 0.5 \frac{e}{C_L+C_R}$. (a) $R_R = 2R_L$. (b) $V = 2 \frac{e}{C_L+C_R}$.

Q_G . The steady state solution for Q_G would satisfy

$$Q_G = \langle Q_n \rangle_{Q_G} \quad (\text{A.3})$$

This equation can have multiple solutions for a given V . In that case, it is possible to get hysteresis in the $I - V$ curve. To understand the conditions for hysteresis, we write Eq. A.3 in terms of U , the electric potential on our single island. Using Eq. 7, 8 we get

$$\langle U \rangle_{Q_G} = V_G - \frac{Q_G}{C_G} \quad (\text{A.4})$$

This is the same as requiring that, for a steady state, the average current through R_G would vanish.

Both sides of Eq. A.4 are plotted in Fig. A.2. Hysteresis is possible if this equation has multiple solutions. This is more likely for large C_G , when the linear function in the RHS of Eq. A.4 has a smaller slope. The exact condition is

$$C_G > \left(\max_{Q_G} \left[-\frac{\partial \langle U \rangle_{Q_G}}{\partial Q_G} \right] \right)^{-1} \quad (\text{A.5})$$

since otherwise the linear function $V_G - \frac{Q_G}{C_G}$ (purple curves in fig. A.2) decreases faster than $\langle U \rangle_{Q_G}$ anywhere, and thus crosses it only once (e.g. green curves in fig. A.2). Analysis of $\langle U \rangle_{Q_G}$ for small voltages, such that only 2 states are possible, shows that we will get hysteresis for

$$C_G > (C_L + C_R) \left[\frac{1}{1 - \frac{R_{\min} (C_L + C_R) V}{R_{\max} e}} - 1 \right] \quad (\text{A.6})$$

We can rewrite this, to get a condition for V :

$$V \frac{C_L + C_R}{e} < V^{hyst} \frac{C_L + C_R}{e} = \frac{R_{\max}}{R_{\min}} \frac{C_G}{C_{\Sigma}} \quad (\text{A.7})$$

As seen in Fig. A.2(a), for small V (blue curve), we have more than one steady state solution. For larger V (orange curve) there is only one solution. For even larger V (green curve), more states become available (more carriers can tunnel to, or from, the island) and $\langle U \rangle_{Q_G}$ becomes, approximately, Q_G independent. This convergence is slower when the ratio R_{\max}/R_{\min} is bigger, as shown in fig. A.2(b). For $R_L = R_R$ (orange curve), $\langle U \rangle_{Q_G}$ is almost Q_G independent for $V = 2 \frac{e}{C_L+C_R}$. For $R_R > R_L$, and the same voltage (green and red curves), $\langle U \rangle_{Q_G}$ becomes more similar to the result for low voltages (blue curve in fig. A.2a). Therefore, we will see a more pronounced hysteresis for small voltages and large resistance ratio.